

Modeling performance of a two-dimensional capsule in a microchannel flow: Long-term lateral migration

Hua Li* and Gang Ma

School of Mechanical and Aerospace Engineering, Nanyang Technological University, Singapore 639798, Singapore

(Received 28 October 2009; revised manuscript received 11 May 2010; published 10 August 2010)

The long-term lateral migration of a two-dimensional elastic capsule in a microchannel is studied numerically in this paper. The numerical method combines a finite volume technique for solving the fluid problem with a front tracking technique for capturing and tracking the capsule membrane. The capsule is modeled as a liquid medium enclosed by a thin membrane which has linear elastic properties. The capsule, whose initial shape is circle and which starts from a near-center position or a near-wall position, experiences tilting and membrane tank-treading, and migrates laterally when moving along the surrounding flow. The lateral migration demonstrates the existence of lift effect of surrounding flow on moving capsule. Before capsule approaches to the microchannel centerline closely, lower membrane dilation modulus and lower viscosity ratio tend to result in faster lateral migration. The initial position also influences the performance behavior of capsule, despite the lateral migration of capsule is a quasisteady process. Small difference in capsule behavior when capsule is not near to the microchannel centerline might lead to significant difference in capsule behavior when capsule approaches closely to the centerline. When capsules are near to microchannel wall, the effect of the wall on capsule behavior might dominate, leading to relatively faster lateral migration. When capsules are not far from microchannel centerline, the effect of the nonlinearity of Poiseuille flow might dominate, resulting in relatively slower lateral movement. When capsules are located closely to the centerline, they behave differently, where the reason still remains poorly understood and it will be one of our future studies. The comparison between the capsule behavior from the present simulation and that by the migration law proposed by Couplier *et al.* [*Phys. Fluids* **20**, 111702 (2008)] shows that the behavioral agreement for near-wall capsule is better than that for near-center capsule, and the best agreement occurs to the near-wall capsule with intermediate membrane dilation modulus and highest viscosity ratio.

DOI: [10.1103/PhysRevE.82.026304](https://doi.org/10.1103/PhysRevE.82.026304)

PACS number(s): 47.15.Rq, 47.11.-j, 87.16.A-, 83.50.Ha

I. INTRODUCTION

The behavior of red blood cells flowing in blood vessels or small tubes has been studied experimentally [1], theoretically [2], or numerically [3] because it is important in physiology. Vesicles have also been investigated [4] because of their extensive use in cosmetic, pharmaceutical or agricultural industries, and they can be used as model systems for studying the properties of red blood cells. Red blood cell and vesicle are examples of capsules that consist of a liquid internal medium enclosed by a thin deformable membrane. Regarding the physical property of the membrane, a capsule may serve as a model for a number of particles. Both red blood cell and vesicle are capsules with an inextensible lipid bilayer membrane, but the red blood cell membrane has an in-plane shear elasticity by virtue of its cytoskeleton. When capsules move in microchannel flow, they undergo hydrodynamic stress and experience deformation. The mechanical behaviors of single red blood cells through microcapillaries are relevant to the rheological properties of blood in microcirculation and even to the overall hydrodynamics of large-scale blood flow [5]. Hence, it is of great importance to develop a suitable physical model to analyze the behavior of capsules in microchannel flow, and understanding the dynamics of individual capsule under different conditions is the first step in studying the rheological properties of capsule suspension.

Some numerical methods have been proposed for studying the behavior of capsule in micro flow. When analyzing problem of tightly fitting particles, where a thin film of liquid exists between the particle and the capillary wall, a lubrication method can be used to model the flow in the narrow gaps [2,6,7]. Boundary integral method for Stokes flow is another popular method for analyzing the behavior of capsule in flow [3,8,9]. Some techniques have been proposed to track the position and motion of arbitrarily shaped interfaces, including capsule membrane, and they can be classified into volume tracking [10,11] and front tracking methods [12,13]. Higher computational accuracy in capsule motion simulation can be achieved by using the front tracking methods, in which the interface itself is represented by a set of additional points [12], while the fluid problem is solved on a stationary grid.

The lateral behavior of capsule in micro flow is an important research area attracting great attention, which can be classified into two groups. One is concerned to the influence of shear flow on the behavior of capsule near to or even adhesive to a wall. Lorz *et al.* [4] experimentally studied the deformation and unbinding of weakly adhering giant vesicle subject to hydrodynamic shear force, and the lift force was found to be large enough to lift the vesicle off the wall. Abkarian *et al.* [14] investigated the motion of binding flaccid vesicle in a linear shear flow by light microscopy, through which a progressive tilt and a transition of unbinding of vesicle were evidenced upon increasing the shear rate, disclosing the existence of a viscous lift force. Sukumaran

*Corresponding author; lihua@ntu.edu.sg

and Seifert [15] employed a boundary element method for analyzing the dynamics of three-dimensional fluid vesicle in steady shear flow at low Reynolds numbers in the vicinity of a wall. The viscous lift force estimated numerically by Sukumaran and Seifert [15] agreed well with the experimental results by Lorz *et al.* [4]. Based on a theoretical study, Cantat and Misbah [16] showed that a vesicle in shear flow experienced a lift force, which was of purely viscous nature and originated from upstream-downstream asymmetry. Seifert [17] theoretically investigated the motion of bound vesicle in shear flow by combining a lubrication analysis of the bound part with a scaling approach to the global motion, and found that a minor inclination of the bound part led to significant lift of vesicle due to the additive effects of lateral and tank-treading motions.

The other group is concerned to the lateral movement of capsule in microchannel flow. Olla [18] theoretically analyzed the behavior of a spheroid vesicle in a plane shear flow bounded from one side by a wall, and found that the tank-treading motion produced a transverse vesicle drift away from the wall. Callens *et al.* [19] studied the dynamics of a vesicle suspension in a shear flow between two parallel walls under microgravity conditions, and concluded that the vesicle was pushed away from the walls due to the presence of the parallel walls. The motion of deformable capsule with small inertia in a plane Poiseuille flow was studied by Dodd and Bagchi [20] based on three-dimensional numerical simulation, from which the lateral migration of capsule toward the channel centerline was observed. Kaoui *et al.* [21] used a boundary integral model to investigate the lateral migration of a suspended vesicle in an unbounded two-dimensional Poiseuille flow in the low Reynolds number limit, and found that the interplay between the nonlinear characteristic of the Poiseuille flow and the vesicle deformation caused the cross-streamline migration of vesicle toward the flow center. Couplier *et al.* [22] experimentally and numerically investigated the cross-streamline noninertial migration of a vesicle in a bounded Poiseuille flow, in which the effect of the walls coupled with the curvature of the velocity profile induced a vesicle movement toward the channel center. Danker *et al.* [23] theoretically studied the effect of the ratio of the inner over the outer fluid viscosities on vesicle behavior, and predicted the coexistence of two types of shapes at centerline. In order to understand why red blood cells (RBCs) move with an asymmetric or slipperlike shape in small blood vessels, Kaoui *et al.* [24] discovered that the adoption of a slipper shape provides higher flow efficiency for RBCs.

The lateral migration of two-dimensional (2D) capsule in microchannel with Poiseuille flow is studied numerically in the present work, where three factors are taken into consideration, namely the initial capsule position, the membrane elastic dilation modulus, and the viscosity ratio which is defined as the ratio of viscosity of fluid inside the capsule membrane to that of fluid outside the membrane. This paper is organized as follows. Details of the governing equations, the nondimensionalization of equations, the treatment of discontinuities in fluid properties across the capsule membrane, the derivation of interaction between capsule membrane and fluid, and the simulation conditions are described in Sec. II. The numerical results corresponding to different initial cap-

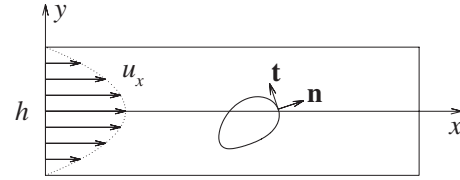


FIG. 1. Schematic illustration of a 2D microchannel with a moving capsule.

sule positions, membrane dilation moduli, and viscosity ratios are presented and discussed with comparison with other available data in Sec. III. Finally, conclusions drawn from this study are summarized in Sec. IV.

II. MODEL AND METHOD

A. Model and governing equations

The lateral migration of 2D capsule in microchannel flow is studied numerically in this paper. The schematic illustration of a 2D microchannel with a moving capsule is shown in Fig. 1, in which h is the height of the microchannel and (x, y) are the coordinates. The microchannel is composed of two walls at the upper and lower boundaries. The x axis coincides with the horizontal line at half height of the microchannel which is termed the centerline. The surrounding fluid, which is outside the capsule membrane, flows from left to right along positive x direction. Its unperturbed velocity field is defined using the 2D Poiseuille profile, which is symmetric with respect to the centerline. The x and y components of the 2D Poiseuille velocity profile are expressed as

$$u_x = 1.5U_m[1 - y^2/(0.5h)^2], \quad u_y = 0, \quad (1)$$

where U_m is the mean velocity, equal to two thirds the velocity at the centerline. A 2D capsule is represented by a closed curve in Fig. 1, with \mathbf{t} being the unit tangent vector pointing in the anticlockwise direction of increasing arc length l , and \mathbf{n} the unit normal vector.

The fluids inside and outside capsule membrane are treated as incompressible, and thus the mass conservation equation is written in the following form:

$$\nabla \cdot \mathbf{u} = 0. \quad (2)$$

In the presence of capsule, the material properties, density and viscosity, of the fluid phases inside and outside capsule membrane are unnecessarily the same. Here, one set of governing equations, Navier-Stokes equations, is solved in the whole computational domain by treating different phases as one fluid with variable material properties. The Navier-Stokes equations are given as

$$\frac{\partial(\rho\mathbf{u})}{\partial t} + \nabla \cdot \rho\mathbf{u}\mathbf{u} = -\nabla p + \nabla \cdot [\mu(\nabla\mathbf{u} + \nabla^T\mathbf{u})] + \mathbf{F}, \quad (3)$$

where ρ and μ are the density and viscosity of fluid, respectively, p the pressure in fluid, \mathbf{u} the fluid velocity vector, t the time, and \mathbf{F} the body force acted on fluid by capsule membrane. The detailed derivation of the body force, \mathbf{F} , will be discussed in Sec. II C.

The following nondimensional variables are introduced:

$$\begin{aligned} x^* &= \frac{x}{x_0}, & u^* &= \frac{u}{U_m}, & \rho^* &= \frac{\rho}{\rho_l}, & \mu^* &= \frac{\mu}{\mu_l}, & t^* &= \frac{t}{x_0/U_m}, \\ p^* &= \frac{p}{\rho_l U_m^2}, \end{aligned} \quad (4)$$

where x_0 is the maximum diameter of the initial shape of capsule, ρ_l and μ_l the density and viscosity of the surrounding fluid, and x_0 , U_m , ρ_l , μ_l , x_0/U_m , and $\rho_l U_m^2$ are the characteristic variables for nondimensionalization. The nondimensionalized Navier-Stokes equations are obtained as

$$\frac{\partial(\rho\mathbf{u})}{\partial t} + \nabla \cdot \rho\mathbf{u}\mathbf{u} = -\nabla p + \frac{1}{R_e} \nabla \cdot [\mu(\nabla\mathbf{u} + \nabla^T\mathbf{u})] + \mathbf{F}, \quad (5)$$

in which the superscript $*$ is omitted for convenience. The nondimensional Reynolds number is defined as follows:

$$R_e = \rho_l U_m x_0 / \mu_l. \quad (6)$$

The numerical method used in the present paper combines a finite volume technique for solving the fluid problem with the front tracking technique proposed by Unverdi and Tryggvason [13] for capturing and tracking the capsule membrane. A regular Eulerian grid is used to discretize the 2D computational domain of the microchannel. The capsule membrane is discretized and represented by a group of Lagrangian nodes, and the straight segments connecting successive Lagrangian nodes are the membrane elements. This method has been adopted to study the initial motion of capsule just after release in microchannel flow [25]. A similar method was used to simulate the procedure of bubble rising [26], and the results demonstrated that the algorithm was robust in flow regimes with large ranges of Reynolds number, and density and viscosity ratios.

B. Treatment of the discontinuities across membrane

The properties, density and viscosity, of the fluids inside and outside capsule membrane may be different in the presence of capsule, and the abrupt jumps in property values exist across the membrane. The variations in properties in computational domain are considered in simulation, and their values are calculated according to the membrane position. We use b to stand for either fluid density or viscosity. To treat the discontinuities, the field distributions $b(\mathbf{x}, t)$ of material properties over the whole computational domain at time t are reconstructed as follows:

$$b(\mathbf{x}, t) = b_2 + (b_1 - b_2) \cdot I(\mathbf{x}, t), \quad (7)$$

where b_1 and b_2 are property values in the first (inside the membrane) and the second (outside the membrane) fluid phases, and $I(\mathbf{x}, t)$ [13] is called the indicator function, which has values of unity and zero in the first and second fluid phases, respectively. The indicator function can be written in form of an integral over the capsule domain $\Omega(t)$ with interface $\Gamma(t)$, where in fact is the position of the capsule membrane

$$I(\mathbf{x}, t) = \int_{\Omega(t)} \delta(\mathbf{x} - \mathbf{x}') d\mathbf{x}', \quad (8)$$

where $\delta(\mathbf{x} - \mathbf{x}')$ is the Dirac-delta function that has a value of infinite when $\mathbf{x}' = \mathbf{x}$ and zero elsewhere. The value of the integral [Eq. (8)] is unity when \mathbf{x} is contained in $\Omega(t)$ and zero otherwise. Taking the gradient of the indicator function and transforming the area integral into an integral over the interface yields

$$\nabla I = \int_{\Gamma(t)} \mathbf{n} \delta(\mathbf{x} - \mathbf{x}') ds. \quad (9)$$

Let $\mathbf{G}(\mathbf{x}, t)$ be the gradient of the indicator function. Taking the divergence of Eq. (9) leads to

$$\nabla^2 I = \nabla \cdot \int_{\Gamma(t)} \mathbf{n} \delta(\mathbf{x} - \mathbf{x}') ds = \nabla \cdot \mathbf{G}. \quad (10)$$

By solving the above Poisson equation, in which the right-hand side is a function of known membrane shape and position at time t , the indicator function $I(\mathbf{x}, t)$ can be reconstructed. The distributions of fluid properties can then be calculated by Eq. (7).

Unverdi and Tryggvason [13] proposed a front tracking method, in which capsule membrane is considered to have a finite thickness instead of zero thickness. The artificial thickness of the membrane depends on the size of the Eulerian grid and is maintained constant during computation. This is realized by using a distribution function $D(\mathbf{x})$ to approximate the Dirac-delta function. This distribution function determines the fraction of quantity distributed to nearby grid points across the artificial thickness of the membrane. In the present work, the following distribution function [27] is used for the 2D grid system

$$D(\mathbf{x} - \mathbf{x}_f) = D_1(x - x_f) D_2(y - y_f), \quad (11)$$

where the distribution function $D_1(x)$ is given as follows:

$$D_1(x) = \begin{cases} \frac{1}{4h_x} \left(1 + \cos \frac{\pi x}{2h_x} \right) & \text{for } |x| \leq 2h_x, \\ 0 & \text{elsewhere} \end{cases}, \quad (12)$$

where h_x is the grid size in x direction. The function $D_2(y)$ is similar to Eq. (12) with y and the grid size in y direction h_y instead of x and h_x . The use of $D(\mathbf{x})$ leads to the following discretized form of the gradient function $\mathbf{G}(\mathbf{x}, t)$,

$$\mathbf{G}(\mathbf{x}, t) = \sum_f D(\mathbf{x} - \mathbf{x}_f) \mathbf{n}_f \Delta s_f, \quad (13)$$

where \mathbf{n}_f is the unit normal vector of the membrane element whose length is Δs_f and center is \mathbf{x}_f . Thus, the sharp jump of the indicator function across the capsule membrane is spread out over the nearby grid points, leading to smooth and continuous change of fluid properties from one side of the capsule membrane to the other side. Hence, this method does not have numerical diffusion across the membrane.

During simulation, the membrane position is advected explicitly using the velocity interpolated from fluid velocities on nearby Eulerian grid points. By using the distribution

function (11) in stead of the δ function to calculate the membrane velocity during interpolation, numerical diffusion can be avoided and the capsule membrane can be captured.

C. Interaction between capsule membrane and fluid

The body force \mathbf{F} in Eq. (3), which reflects the interaction between capsule membrane and surrounding fluid, can be deduced by the equilibrium of membrane. The vectorial tension exerted on a 2D membrane is given by

$$\mathbf{T} = \boldsymbol{\tau} + q\mathbf{n}, \quad (14)$$

where τ is the in-plane tension, and q the transverse tension. The membrane load, which is the discontinuity in surface traction across the membrane, can be obtained through a force balance over an infinitesimal section of the membrane [28], and is given by

$$\Delta\mathbf{f} = \Delta f^n \mathbf{n} + \Delta f^t \mathbf{t} = -\frac{d\mathbf{T}}{dl} = -\frac{d}{dl}(\boldsymbol{\tau} + q\mathbf{n}). \quad (15)$$

Using the derivative relations, $d\mathbf{t}/dl = -\kappa\mathbf{n}$ and $d\mathbf{n}/dl = \kappa\mathbf{t}$, where κ is the curvature of capsule membrane, and the expression of transverse shear tension in terms of bending moment $q = dm/dl$, one has the following normal and tangential membrane loads:

$$\Delta f^n = \kappa\tau - \frac{d^2m}{dl^2}, \quad \Delta f^t = -\frac{d\tau}{dl} - \kappa\frac{dm}{dl}. \quad (16)$$

In the present study, capsule is modeled as a liquid medium enclosed by a thin membrane which has linear elastic properties. Let E_M and E_B be the area elastic dilation modulus and the bending stiffness of membrane, respectively, the in-plane tension is expressed as $\tau = E_M \varepsilon$, where ε is the tensile strain of membrane, and the bending moment is $m = E_B \Delta\kappa = E_B (\kappa - \kappa_0)$ where κ_0 is the resting curvature of membrane. The equilibrium equations can thus be expressed as

$$\Delta f^n = E_M \kappa \varepsilon - E_B \frac{d^2\kappa}{dl^2}, \quad \Delta f^t = -E_M \frac{d\varepsilon}{dl} - E_B \kappa \frac{d\kappa}{dl}. \quad (17)$$

The concentrated force acted on membrane by fluid and defined on membrane nodes, \mathbf{F}_{node} , can be calculated by integrating the membrane load characterized by Eq. (17). The concentrated force acted on fluid by membrane and defined on membrane nodes is

$$\mathbf{F}_{\text{fluid}} = -\mathbf{F}_{\text{node}}. \quad (18)$$

The body force \mathbf{F} in Eq. (3) which is acted on fluid and defined on fluid grid points can be calculated based on the knowledge of $\mathbf{F}_{\text{fluid}}$. By using the distribution function (11), the concentrated force defined on membrane nodes, $\mathbf{F}_{\text{fluid}}$, is smoothed and distributed to nearby fluid grid points through

$$\mathbf{F}(\mathbf{x}, t) = \sum_f D(\mathbf{x} - \mathbf{x}_f) \mathbf{F}_{\text{fluid}}. \quad (19)$$

According to the nondimensionalization approach used in the present paper, area dilation modulus and bending stiffness, which describe the mechanical properties of membrane, are nondimensionalized as

$$E_m = E_M / (\rho_l U_m^2 x_0), \quad E_b = E_B / (\rho_l U_m^2 x_0^3). \quad (20)$$

D. Simulation conditions

The lateral migration of 2D capsule in microchannel flow is studied numerically in the present study, where three factors are considered, i.e., the initial capsule position, the membrane elastic dilation modulus, and the viscosity ratio, r_v , which is defined as the ratio of viscosity of fluid inside capsule membrane to that of fluid outside the membrane. Pozrikidis [3] numerically studied the dependence of the behavior of red blood cell on a nondimensional variable, $G = \mu U_m / E_s$, where μ is the viscosity of surrounding liquid, U_m the mean velocity of axisymmetric Poiseuille flow, and E_s the membrane shear modulus, and the results were interpreted as affected by the mean velocity. If μ and U_m are kept constant, the effects of membrane mechanical properties and viscosity ratio on capsule behavior can be elucidated. Throughout the present paper, unless otherwise mentioned, length is expressed in unit of x_0 , time in unit of x_0 / U_m , velocity in unit of U_m , and membrane dilation modulus in unit of $\rho_l U_m^2 x_0$.

The nondimensional y coordinate of computational domain ranges from -1.2 to 1.2 , i.e., the height of microchannel is 2.4 . Generally, long computational domain is chosen if long-term capsule behavior is required. However, the simulation on large computational domain is quite time consuming. In order to solve this problem, short computational domain is chosen in this paper and a modification on the domain is adopted during simulation for obtaining long-term capsule behavior. The nondimensional x coordinate of the initial computational domain ranges from 0 to 6 , i.e., the length of computational domain is 6 . The size of 120×48 is chosen for the Eulerian grid, i.e., one unit length is meshed with 20 grids. It is known that the effect of the left or right end of the computational domain on capsule behavior can be ignored if the nondimensional distance between the capsule center and either of the two ends is not less than 2.0 [25]. In the present work, only a single capsule is considered in each of the simulations. At the start of simulation, a capsule with zero speed is released in the flow just like that the capsule appears all at once in the unperturbed background flow, and the nondimensional distance between the capsule center and the left end of the computational domain is chosen to be 2.5 in the present study. The capsule moves rightward with surrounding flow after release. The position of capsule is checked once every 10^3 time steps during simulation. If the capsule center is located less than 2.5 to the right end, the computational domain will be moved in positive x direction over a distance, such that the capsule center is near to but not less than 2.5 to the left end of the new computational domain. During the modification, the length of the computational domain is kept constant, and the computed values, such as density and velocity, are transferred accordingly. Let us consider a transfer length of l_t . In order to realize this transfer, the value of a mechanical variable f is required to be modified through the following approach:

TABLE I. Values of nondimensional membrane dilation moduli (E_m) and viscosity ratios (r_v) for all the cases.

Case No.	Case type	E_m	r_v
NC01	Near-center	500	1.0
NC02		2500	0.2
NC03		2500	1.0
NC04		2500	5.0
NC05		10000	1.0
NW06	Near-wall	500	1.0
NW07		2500	0.2
NW08		2500	1.0
NW09		2500	5.0
NW10		10000	1.0

$$\begin{cases} f_{new}(x,y) = f_{old}(x+l_t,y), & 0 \leq x \leq L_x - l_t \\ f_{new}(x,y) = f_{old}(L_x,y), & L_x - l_t < x \leq L_x \end{cases}, \quad (21)$$

where $f_{old}(x,y)$ and $f_{new}(x,y)$ are values of f at position (x,y) in the old and new computational domains, respectively, and L_x is the length of computational domain in x direction. After the computational domain is modified in this way, computation is carried out continuously. This kind of boundary condition is different from the periodic one. For both boundary conditions, the velocities of flow particles on the left boundary are the same as those of corresponding particles on the right boundary. In the present simulation, the y components of velocities of these particles always remain to be zero, while in the periodic boundary condition, it is unnecessary for the y components of velocities to be zero.

The initial capsule shape is circle, and this initial shape is also used as the resting shape. The capsule membrane is represented and discretized by 200 Lagrangian nodes. Two kinds of initial capsule center positions are considered. The first is located at $(2.5, -0.1)$, i.e., 0.1 unit length lower than the centerline, and the corresponding simulation case is termed the near-center case. The second kind of simulation case is termed the near-wall case, in which the capsule center starts from $(2.5, -0.5)$, i.e., 0.5 unit length lower than the centerline and only 0.2 unit length between the capsule lowest point and the bottom boundary. For each initial capsule position, three nondimensional membrane dilation moduli, 500, 2500, and 10000, are used as input in simulations. When nondimensional membrane dilation modulus is 500 or 10000, only one viscosity ratio, 1.0, is taken into consideration, while when nondimensional membrane dilation modulus is 2500, three viscosity ratios, 0.2, 1.0, and 5.0, are considered to elucidate the effect of viscosity ratio on capsule motion. Totally this paper carries out ten simulations, numbered in Table I with corresponding membrane dilation moduli and viscosity ratios.

Simulations are conducted at Reynolds number of 0.01, and at density ratio of the internal fluid to the external fluid of 1.098 [29]. In the present case studies, the influence of gravity is not considered despite there is a density difference. The ratio of the reduced bending stiffness to the reduced

dilation modulus, $E_b/E_m = 1 \times 10^{-5}$. In this paper, the size of computational domain, the initial capsule shape, and the resting capsule shape have been specified. For given ρ_l , x_0 , and U_m , the effect of membrane elastic property and viscosity ratio on capsule behavior can be analyzed. If ρ_l , x_0 , and E_M are specified, and R_e [Eq. (6)] is constant, the effect of mean velocity or viscosity of surrounding liquid on capsule behavior can be elucidated, similar to the study in [3].

III. RESULTS AND DISCUSSION

A. Results

1. Near-center capsule

Evolutions of the center position in y direction, and the center velocities in y and x directions, v_y and v_x , of near-center capsule are shown in Figs. 2(a)–2(c), respectively. One important feature of the off-center capsule flowing in microchannel with walls is the lateral migration of capsule away from the walls. The lateral migration shown in Fig. 2(a) indicates the existence of lift effect of surrounding flow on moving capsule. Capsule velocity, v_y , increases rapidly in the period from the beginning to nondimensional time of 1–2, during which v_x decreases rapidly. This period is actually an adjustment procedure and is termed the initial adjustment period. After the initial adjustment period, v_y becomes stable for a certain period as shown in Fig. 2(b), i.e., capsule moves toward the centerline approximately linearly with time as shown in Fig. 2(a). Capsule deformation can be characterized by morphological properties, which are determined based on the calculations of the zero-, first-, and second-order moments of capsule shape, as proposed by Dunn and Brown [30]. Three dimensionless morphological measures, namely, extension, dispersion and orientation, are calculated by considering the information of whole capsule shape [25]. Extension, m_{ext} , measures how much a 2D shape differs from a circle, and it equals to zero when the shape is circular and increases without limit as the shape becomes less compact. Dispersion, m_{dis} , quantifies the difference between a 2D shape and its equimomental ellipse. Dispersion is zero if the shape is an ellipse, and it increases with the irregularity of the shape. Orientation, m_{or} , is the angle formed by the semi-major axis of the equimomental ellipse with respect to positive x direction. Variations of extension, dispersion, and orientation of near-center capsule are shown in Fig. 2(d)–2(f), respectively. In the initial adjustment period, capsule is subject to large dynamic force, and deforms quickly, as observed from the curves of extension and dispersion in Fig. 2(d) and 2(e), respectively.

In many circumstances, capsule membrane undergoes tank-treading motion. To clearly show the membrane motion, a representative point is specified on capsule membrane. The initial position of the representative point of the initially circular capsule considered in this paper is at the right end of diameter parallel to the centerline, i.e., $(3.0, -0.1)$ in near-center case and $(3.0, -0.5)$ in near-wall case. A parameter, a_{tr} , is defined as the angle formed by the line, starting from capsule centroid and ending at representative point, with respect to x direction. The schematic illustration of a capsule

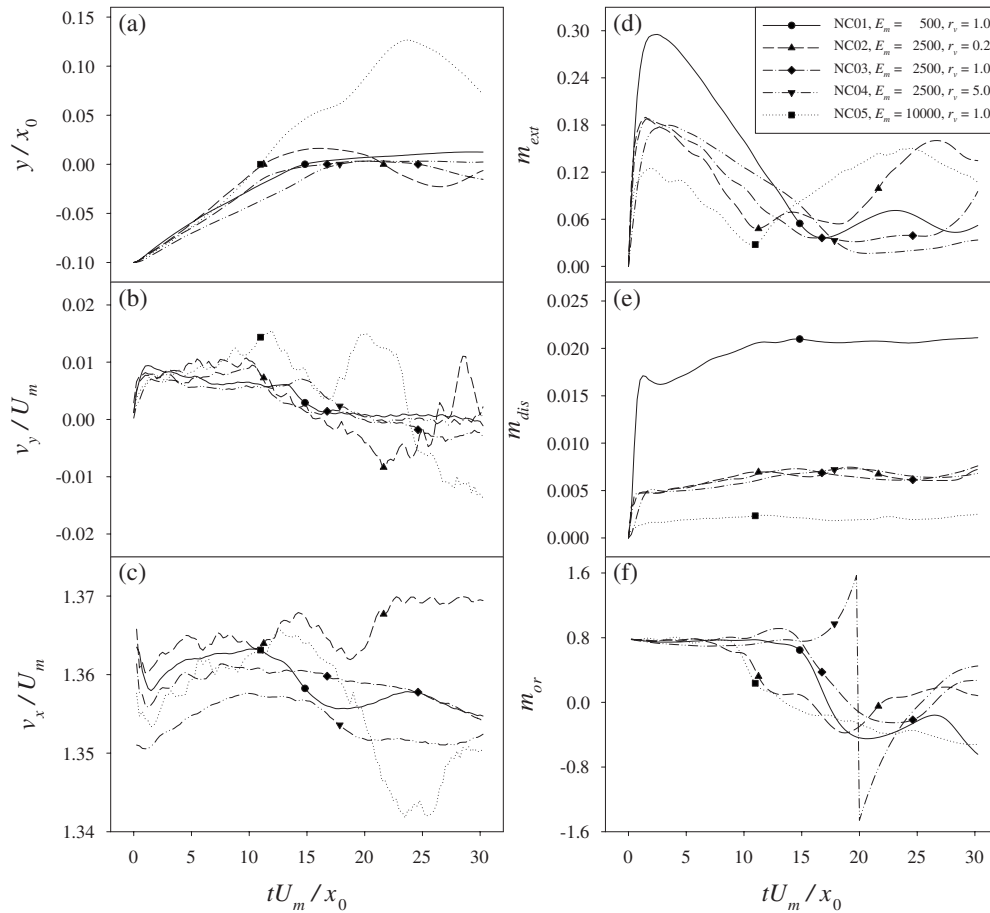


FIG. 2. Evolution of the center position in y direction (a), the center velocity in y direction (b), the center velocity in x direction (c), the extension (d), the dispersion (e), and the orientation (f) of the near-center capsule. The time, at which the capsule centroid coincides with the centerline, is obtained through interpolation and is represented by symbol in (a), and corresponding points are also shown in (b)–(f).

with its representative point and angle a_{tt} is shown in Fig. 3. Figure 4 shows the evolution of position and shape of the capsule in near-center case of NC03, termed the NC03 capsule, with nondimensional membrane elastic dilation modulus of 2500 and viscosity ratio of 1.0. Nondimensional time is shown by the number on top of corresponding capsule snapshot represented by a closed curve, on which a dot is used to show the position of representative point. It is seen from Fig. 4 that the front/downstream end of capsule bulges

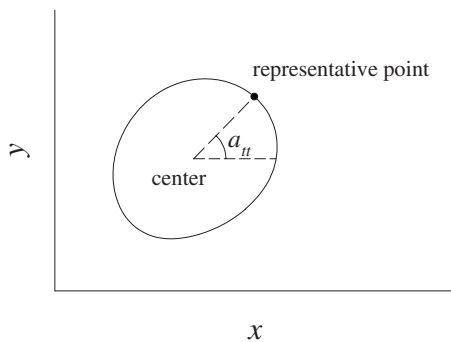


FIG. 3. Schematic illustration of a capsule with representative point, and the definition of angle a_{tt} , which shows the motion of membrane.

while the rear/upstream end becomes less convex, showing more or less similar parachute shape predicted for capsule [8] and red blood cell [3]. The deformation is undergone by capsule due to the hydrodynamic stresses imposed by surrounding Poiseuille flow on capsule membrane. Through the movement of the representative point, Fig. 4 qualitatively shows the membrane tank-treading motion of near-center capsule, which is not marked because the capsule is near to the centerline, i.e., the shear gradient to which the capsule is subject is not high. The movement of the representative point of the NC03 capsule illustrated in Fig. 4 shows that the membrane undergoes clockwise tank-treading motion, and the motion slows down with time since the change in position of the representative point with respect to the capsule cannot be observed when the capsule center is near to the centerline. Temporal evolutions of a_{tt} for the near-center capsule are shown in Fig. 5(a). Distributions of membrane tank-treading velocity of the NC03 capsule at nondimensional times of 0.5, 2, 5, 10, and 25, and the NC05 capsule at nondimensional times of 0.5, 2, 5, 17, and 25 are illustrated in Figs. 5(b) and 5(c), respectively.

From each of the curves in Fig. 2(a), the time, at which the capsule centroid coincides with the microchannel centerline, can be obtained through interpolation, and is represented by a symbol on the curve. Corresponding values of v_y ,

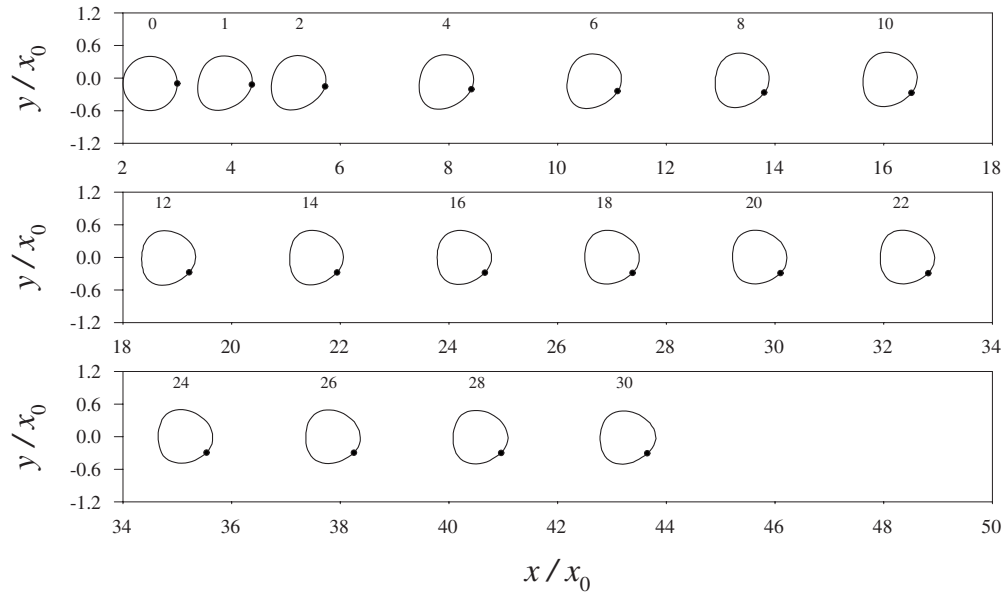


FIG. 4. Evolution of position and shape of near-center NC03 capsule with nondimensional membrane elastic dilation modulus of 2500 and viscosity ratio of 1.0. Number on top of each capsule snapshot indicates the corresponding nondimensional time.

v_x , morphological measures, and a_{tt} at the same time are marked by symbols on corresponding curves in Figs. 2(b)–2(f) and 5(a).

2. Near-wall capsule

Evolutions of the center position in y direction, the center velocities in y and x directions, v_y and v_x , and three morphological measures of near-wall capsule are shown in Figs. 6(a)–6(f). Figure 7 shows the evolution of position and shape of capsule in the near-wall case NW08 with nondimensional membrane elastic dilation modulus of 2500 and viscosity ratio of 1.0. Nondimensional time is given out on top of corresponding capsule snapshot, on which a dot is used to show the position of representative point. The capsule shape changes with time, and becomes nearly symmetric about the microchannel centerline after the capsule center moves near to the centerline at nondimensional time of about 38. It is seen from Fig. 7 that, when the center of the NW08 capsule is near to the centerline, its shape shows similar characteristic to that of the corresponding near-center NC03 capsule shown in Fig. 4, namely the front/downstream end of the capsule bulges and the rear/upstream end becomes less convex. Membrane tank-treading motion of near-wall capsule can be clearly observed from the motion of representative point shown in Fig. 7. The tank-treading motion fades out as capsule moves toward the centerline because of the decrease of shear rate the capsule undergoes. For the NW08 capsule shown in Fig. 7, the representative point turns about half circle from nondimensional time of 0 to about 10, while the tank-treading motion is much slower from time 38 to 50 when the capsule is located near to the centerline. This procedure is represented by the temporal evolution of a_{tt} of the NW08 capsule as shown in Fig. 8, where the temporal evolutions of a_{tt} of all near-wall capsules are demonstrated. From each of the curves in Fig. 6(a), the time, at which the capsule centroid coincides with the microchannel centerline,

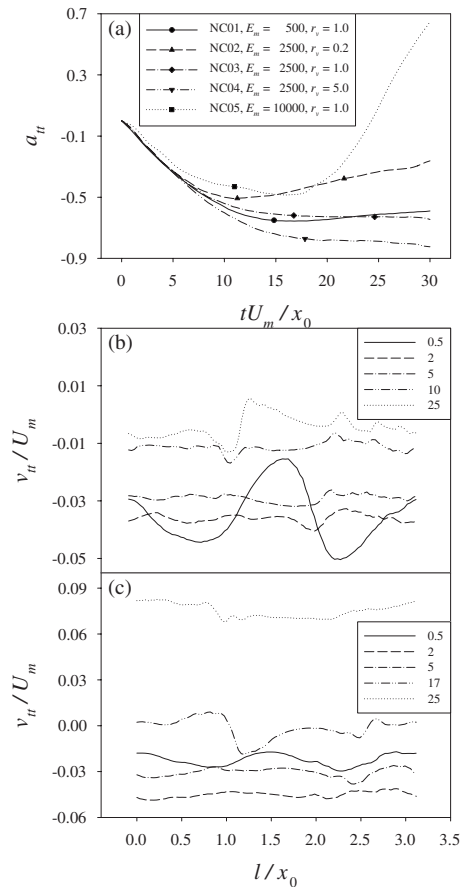


FIG. 5. Temporal evolution of att of the near-center capsule (a), where the value of att in each case at time when the capsule centroid coincides with the centerline is represented by symbol on corresponding curve; the membrane tank-treading velocity distribution of the NC03 capsule at nondimensional times of 0.5, 2, 5, 10, and 25 (b); and the membrane tank-treading velocity distribution of the NC05 capsule at nondimensional times of 0.5, 2, 5, 17, and 25 (c).

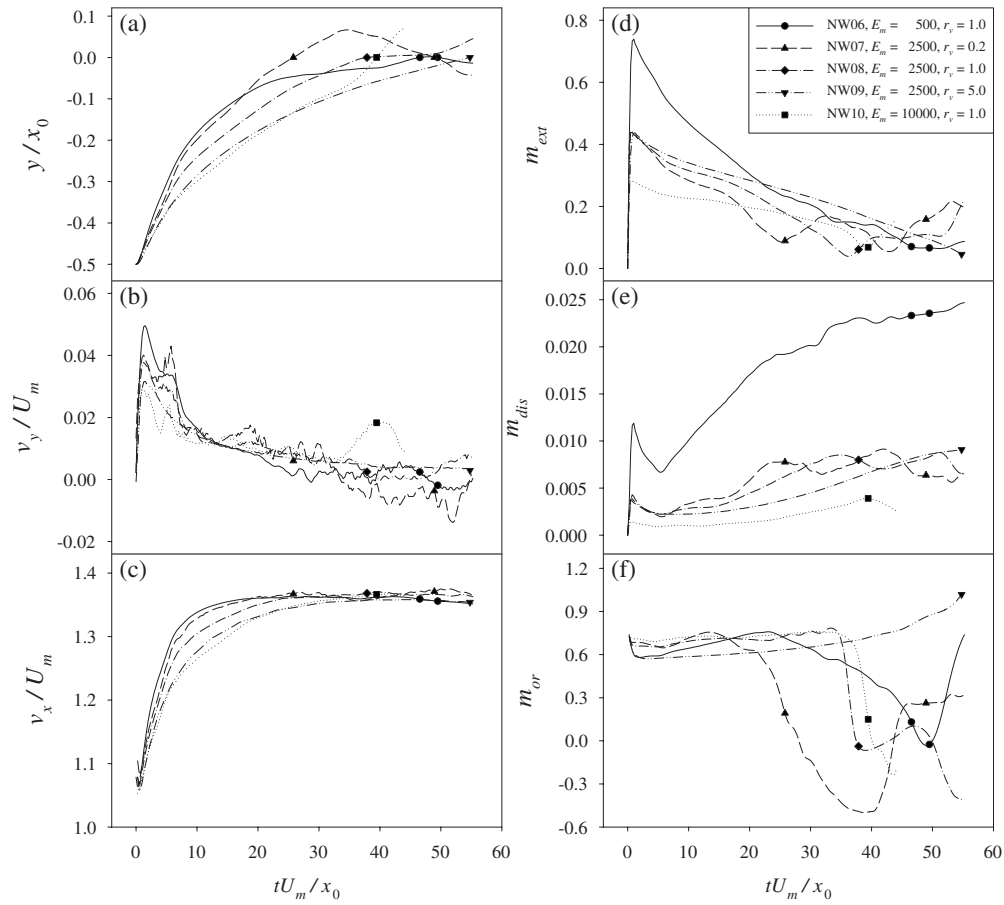


FIG. 6. Evolution of the center position in y direction (a), the center velocity in y direction (b), the center velocity in x direction (c), the extension (d), the dispersion (e), and the orientation (f) of the near-wall capsule. The time, at which the capsule centroid coincides with the centerline, is obtained through interpolation and is represented by symbol in (a), and corresponding points are also shown in (b)–(f).

can be obtained through interpolation, and is represented by a symbol on the curve. Corresponding values of v_y , v_x , morphological measures, and a_{tt} at the same time are marked by symbols on corresponding curves in Figs. 6(b)–6(f) and 8.

B. Discussion

1. Effect of the membrane elastic dilation modulus

The effect of the membrane elastic dilation modulus on behavior of near-center capsule is studied by comparing the results of the NC01, NC03, and NC05 capsules. The behavior of capsule, on one hand, is determined by its mechanical property. The ratio of the reduced membrane bending stiffness to the reduced membrane dilation modulus is fixed in our simulations. Lower membrane dilation modulus together with lower membrane bending stiffness renders capsule with less resistance to flow force, and leads to larger capsule deformation. On the other hand, the behavior of capsule also depends on environmental conditions, such as the presence of a wall, the nonlinearity of the shear flow, and the nonlinear characteristic of surrounding fluid. A capsule does not exhibit a lateral migration with respect to the flow direction in an unbounded linear shear flow in the limit of low Reynolds number. In the presence of a wall, however, a capsule in linear shear flow is found to migrate away from the wall

because of the translational asymmetry perpendicular to the flow direction [16]. Nonlinear characteristic of Poiseuille flow together with capsule deformation causes a cross-streamline migration of capsule toward the centerline even if the Poiseuille flow is unbounded [21]. The nonlinear contribution of term $\nabla \cdot \rho \mathbf{u} \mathbf{u}$ in the Navier-Stokes equations leads to lateral migration of even rigid sphere [31].

The lateral migration behavior of near-center capsule consists of two parts, before it moves across the microchannel centerline, as illustrated in Fig. 2(a). In the first part, namely, just after the initial adjustment period, velocity in y direction v_y does not change much, as shown in Fig. 2(b), and capsule moves almost linearly with time in y direction, as shown in Fig. 2(a). In the second part, when approaching to the centerline closely, different capsules behave differently. In the near-center case, the initial position of capsule is not near to the wall, the effect of wall on capsule behavior is not significant. The lateral migration of capsule results mainly from the combination of the nonlinear characteristics of Poiseuille flow and capsule deformation in the first part. The softer the capsule becomes, the larger deformation is observed, and the more significant interaction with surrounding flow, leading to faster lateral migration. In simulation, capsule is released at the beginning, when the surrounding fluid flow is unperturbed Poiseuille flow, and the capsule has perfect circular

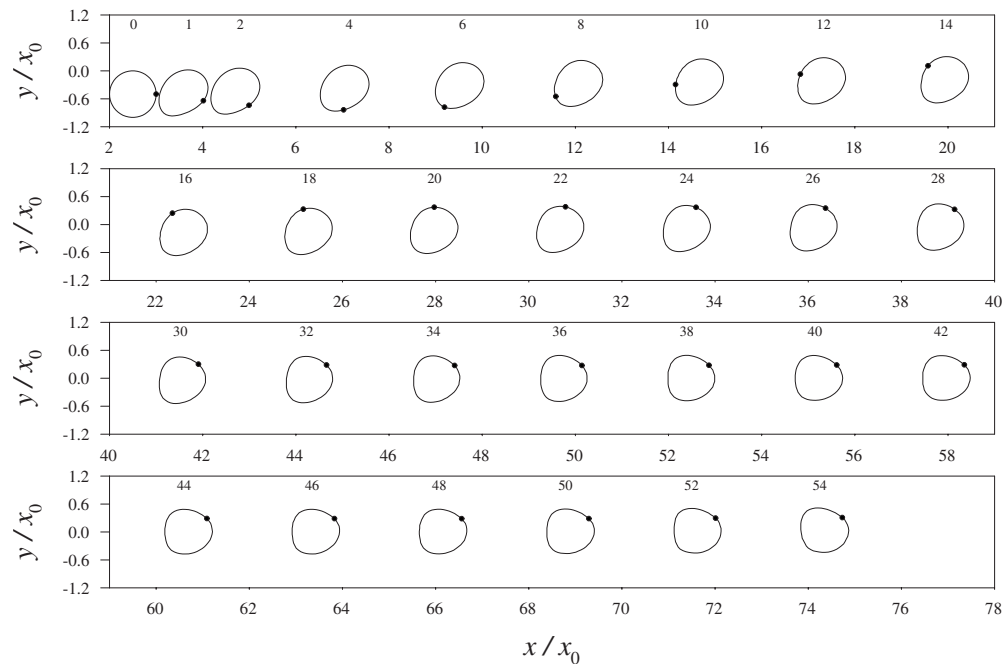


FIG. 7. Evolution of position and shape of the capsule in near-wall case NW08 with nondimensional membrane elastic dilation modulus of 2500 and viscosity ratio of 1.0. Number on top of each capsule snapshot indicates the corresponding nondimensional time.

shape. The capsule and the surrounding flow need to adapt to match each other. Among the NC01, NC03, and NC05 capsules, the NC01 capsule possesses the lowest membrane elastic dilation modulus, and the NC05 capsule the highest one, so the NC01 capsule undergoes the largest deformation with the highest extension and dispersion, while the NC05 capsule has the lowest extension and dispersion in the initial adjustment period, as shown in Figs. 2(d) and 2(e). As expected, the NC01 capsule achieves the fastest lateral migration, while the NC05 capsule the slowest one, from the beginning to nondimensional time of about 5, as shown in Fig. 2(a). The capsule with faster lateral migration is less distant from the centerline, and experiences higher background flow velocity, i.e., having higher v_x , thus, the NC01 capsule moves along x direction with highest v_x , and the NC05 capsule with lowest v_x , as observed from Fig. 2(c). A capsule moving in a shear flow deforms and aligns itself with the

flow. The capsule in the present study starts from the lower half of the microchannel and the background fluid flows from left to right, such that the capsule orientation tends to be positive before the capsule reaches the centerline. As illustrated in Fig. 2(f), orientations of all the near-center capsules are positive and almost the same at the beginning, and remain approximately constant for a period. A capsule moving in a shear flow not only aligns itself with the flow, but experiences membrane tank-treading motion to suit the background flow as well. According to the computational conditions in the present study, capsule needs to undergo clockwise membrane tank-treading motion at the beginning. As seen from Fig. 5(a), a_{tt} of all the near-center capsules decreases, indicating the existence of clockwise tank-treading motion of membrane. Among the three capsules discussed in the present paragraph, the NC05 capsule undergoes the slowest membrane tank-treading motion, while the other two capsules have almost the same membrane motion.

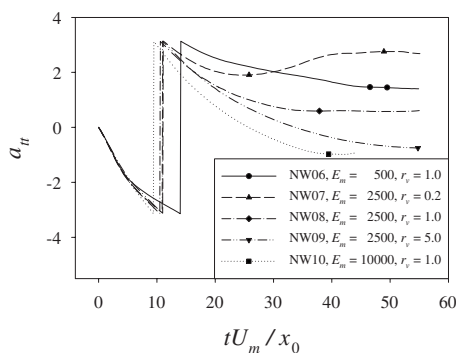


FIG. 8. Temporal evolution of att of the near-wall capsule. The value of att in each case at time when the capsule centroid coincides with the centerline is represented by symbol on corresponding curve.

Figure 2(d) shows that, after the initial adjustment period, capsule undergoes decrease in extension, which might be due to two effects, namely, the membrane elastic properties which make the capsule restore its initial shape, and the decrease of shear gradient to which the capsule is subject to when capsule approaches the centerline. It is seen from Fig. 2(d) that the extension of capsule with lower membrane elastic dilation modulus decreases more rapidly. After reaching local minimum, capsule extension increases again. Figure 2(d) shows that extension is quite low at time when capsule center coincides with the centerline, meaning that capsule experiences less deformation on the centerline. Capsule dispersion does not change much after the initial adjustment period, as shown in Fig. 2(e). With the decrease of capsule deformation and the decrease of distance between capsule center and microchannel centerline, the effect of Poiseuille

flow on capsule behavior might go down. The shear rate to which the capsule is subject to also decreases, leading to the decrease of tank-treading motion of capsule membrane, i.e., the slowing down in the change of a_{tt} , as shown in Fig. 5(a). When capsule approaches closely to the centerline, decrease in v_y occurs to all the near-center capsules except the NC05 capsule which experiences increase in v_y , as shown in Fig. 2(b). After nondimensional time of about 7, position of the NC05 capsule in y direction starts to become higher than those of the other two capsules, because of its faster lateral movement. Therefore, velocity v_x of the NC05 capsule is the highest as seen from Fig. 2(c). When the near-center capsules first move across the centerline, their orientations decrease, meaning that they turn in the clockwise direction. The orientation of the NC05 capsule decreases at nondimensional time of about 8, and that of the NC01 and NC03 capsules decreases at nondimensional time of 14–15. The NC05 capsule migrates continuously after moving across the centerline. After reaching the minimum value, a_{tt} of the NC05 capsule increases, meaning that the membrane motion changes from clockwise to anticlockwise direction, since the capsule has already moved into the upper half of the microchannel. After nondimensional time of about 20, v_x of the NC05 capsule is the lowest among the NC01, NC03, and NC05 capsules because it is located the most distant from the centerline. The NC05 capsule moves downward with negative v_y after reaching the maximum y coordinate. The difference of behaviors between the NC01 and NC03 capsules is not remarkable, as seen from Figs. 2(a) and 5(a).

The effect of the membrane elastic dilation modulus on behavior of near-wall capsule is studied by comparing the results of the NW06, NW08, and NW10 capsules. The lateral migration behavior of the near-wall capsule consists of three parts, before it moves across the microchannel centerline. In the first part, namely, just after the initial adjustment period, the capsule moves toward the centerline with relatively higher velocity, as shown in Fig. 6(b). The subsequent two parts for the near-wall capsule are somewhat similar to the two parts for the near-center capsule. In the near-wall case, capsule center is nearer to microchannel wall at the beginning than that in the near-center case, the lateral migration of capsule is caused mainly by the interaction between microchannel wall and capsule deformation. The nonlinearity of Poiseuille flow also has effect on behavior of the near-wall capsule, but this effect does not dominate. Capsule with lower membrane dilation modulus undergoes higher deformation, and achieves faster lateral migration. The NW06 capsule has the lowest membrane elastic dilation modulus, and the NW10 capsule the highest one, and they experience the largest and the smallest deformation in the initial adjustment period, respectively, as illustrated in Figs. 6(d) and 6(e). The maximum extension of near-wall capsule is larger than that of the corresponding near-center capsule, since the near-wall capsule is subject to higher shear gradient. In the initial adjustment period, the maximum dispersion of near-wall capsule is less than that of the corresponding near-center capsule, which might be because that the near-wall capsule is more prolonged under higher shear gradient, leading to less difference of its shape from its equimomentary ellipse. The NW06 capsule and the NW10 capsule achieves

the fastest and the slowest lateral migrations, respectively, as observed from Fig. 6(a). In the first part, from nondimensional time of 2 to 8, capsule moves upward quickly as illustrated in Fig. 6(a), and v_y decreases apparently as shown in Fig. 6(b). Chaffey *et al.* [32] studied the lateral movement of a droplet in a wall-bounded linear shear flow, and predicted that the lateral velocity decreases inversely with the square of the distance from the wall. The lateral velocity of the capsule in the present study should decrease more rapidly than that in the cases studied by Chaffey *et al.* [32], since the shear rate decreases linearly with the increase of the distance between the capsule center and the wall of microchannel with Poiseuille flow. The capsule with faster lateral migration has less distance from the centerline, and experiences higher background flow velocity, and thus has higher v_x . As observed from Fig. 6(c), the NW06 capsule and the NW10 capsule have the highest and lowest v_x , respectively. Variations of the orientations of the near-wall capsules are different from those of the near-center capsules. The orientation drops in the initial adjustment period, and then increases slowly afterward. In the first part, a_{tt} of all the near-wall capsules decreases, indicating the existence of clockwise tank-treading motion of capsule membrane, and the membrane dilation modulus has insignificant effect on capsule's a_{tt} , as seen in Fig. 8.

In the second part, namely after the nondimensional time of 8–12, the lateral velocity of capsule becomes relatively low, and decreases slowly, such that the lateral movement of capsule slows down, as observed in Fig. 6(a). With the increase of the distance between the capsule and the wall, and the decrease of the distance between the capsule and the centerline, the effect of the wall on capsule behavior decreases, and the effect of the nonlinearity of Poiseuille flow on capsule behavior becomes more important. In this part, the membrane dilation modulus affects the behavior of near-wall capsule in almost the same way as it affects the near-center capsule in the first part. In both the first and second parts, the extension of near-wall capsule decreases, due to the membrane elastic properties which make the capsule restore the initial shape, and because of the decrease of the shear gradient when the capsule approaches the centerline. With the decrease of capsule deformation and the decrease of the distance between the capsule center and microchannel centerline, the effects of both the wall and the nonlinearity of Poiseuille flow goes down. In the third part, the lateral velocities, v_y , of all the near-wall capsules except the NW10 capsule decrease when they approach and move across the centerline. The NW10 capsule, which has the highest membrane dilation modulus, experiences abrupt increase in v_y when its center is located about 0.07 unit length lower than the centerline, as shown in Fig. 6(b), and moves across the centerline with high v_y . This characteristic is quite similar to that of the corresponding near-center NC05 capsule, which has the same mechanical properties as the NW10 capsule. Figure 6(d) demonstrates that the extension of near-wall capsule is quite low when its center coincides with the centerline, meaning that the capsule experiences less deformation on the centerline. After the initial adjustment period, the capsule dispersion first undergoes a short period of decrease, and then increases again in spite of the decrease in capsule ex-

tion, as shown in Fig. 6(e). Generally, the capsule dispersion is at a relatively high level when capsule center is on the centerline, because the difference in convexity between the front/downstream end and the rear/upstream end, shown in Fig. 7, results in apparent difference of capsule shape from its equimomental ellipse.

The results in this subsection show that, before capsule approaches to the microchannel centerline closely, lower membrane dilation modulus tends to result in faster lateral migration of capsule.

2. Effect of the viscosity ratio

The effect of the viscosity ratio on the behavior of near-center capsule is studied by comparing the results of the NC02, NC03, and NC04 capsules. In the first part of the near-center case, the interaction between the nonlinearity of Poiseuille flow and the capsule deformation leads to the lateral migration of capsule. Capsule with lower viscosity ratio deforms faster under the same outside load, and seems to be softer. The interaction between larger deformation of capsule and background Poiseuille flow leads to faster lateral migration. Therefore, the capsule with higher viscosity ratio might behave somewhat similar to that with higher membrane dilation modulus. When the process is slow enough, capsules with the same membrane dilation modulus and different viscosity ratios may behave similarly, while capsules with different membrane dilation moduli behave differently, no matter how slow the process is. The faster the process is, the more significant the effect of the viscosity ratio on the behavior of capsule. Among the NC02, NC03, and NC04 capsules, the NC02 capsule, which has the lowest r_v , undergoes the fastest deformation, and the NC04 capsule, which has the highest r_v , undergoes the slowest deformation, as seen from Fig. 2(d). As expected, the NC02 capsule and the NC04 capsule experience the fastest and the slowest lateral migration, respectively, as illustrated in Fig. 2(a). Because the NC02 capsule is the closest to the centerline among the three capsules, it is subjected to the highest background flow velocity, and has the highest moving velocity v_x , and the NC04 capsule has the lowest v_x , as illustrated in Fig. 2(c). After the initial adjustment period, the extension of capsule goes down, and Fig. 2(d) shows that the extension of capsule with lower viscosity ratio decreases faster. The dispersion of near-center capsule doesn't change much after the initial adjustment period, and Fig. 2(e) also shows that the viscosity ratio has insignificant effect on the dispersion of the near-center capsule. The orientations of the three capsules are almost the same at the beginning, and remain approximately constant for a period. When the capsules approach to the microchannel centerline, they begin to revolve about their center. The orientations of the NC02 and NC03 capsules decrease at nondimensional time of about 9 and 15, respectively, while that of the NC04 capsule increases at nondimensional time of about 17. Capsule with lower r_v migrates faster laterally, and moves closer to the centerline. As such, it undergoes lower shear rate, namely, it has slower membrane tank-treading motion, as shown in Fig. 5(a).

The effect of the viscosity ratio on behavior of the near-wall capsule is studied by comparing the results of the

NW07, NW08, and NW09 capsules. As discussed above, capsule with lower viscosity ratio moves faster in y direction, which can be observed from Fig. 6(a). It is known from Figs. 6(a)–6(d) that the viscosity ratio influences the behavior of the near-wall capsule in the same way as it does for the near-center capsule.

The results in this subsection indicate that, before capsule approaches to the microchannel centerline closely, lower viscosity ratio tends to bring about faster lateral migration of capsule, showing similar effect as the membrane dilation modulus.

3. Effect of the initial position of capsule

It is observed from the results of the present study that different capsules behave differently when they approach to the centerline closely. For example, the NC03 capsule reaches the upper half of microchannel at nondimensional time of about 16.8, and moves downward and reaches the lower half of microchannel at nondimensional time of about 24.6. Because v_y of the NC03 capsule is very low between the two times when its center coincides with the centerline, the capsule is quite near to the centerline in this period, looking like that it stays on the centerline. The procedure of the lateral migration of the NW06 capsule is similar to that of the NC03 capsule, the difference being that the period during which the NW06 capsule is near to the centerline is shorter than that of the NC03 capsule. Velocity v_y of the NC04 capsule is quite low after its center reaches the centerline, it looks like that the NC04 capsule stays on the centerline after nondimensional time of 17.8. Velocity v_y of the NW08 capsule is very low after it reaches the centerline at about nondimensional time of 37.9 and before it moves upward away from the centerline at time of 48. It looks like that the NW08 capsule stays on the centerline for a period after reaching it, and then moves upward into the upper half of the microchannel. Other capsules move across the centerline one or two times without staying on the centerline. The lateral migration behavior of capsule observed in the present paper is different from the results by Kaoui *et al.* [21] and Couplier *et al.* [22], where they found that the lateral migration velocity of vesicle becomes zero when vesicle reaches the centerline. The nonlinear term $\nabla \cdot \rho \mathbf{u} \mathbf{u}$ in the Navier-Stokes equations was not considered in their studies, which might be the main reason for the difference in results.

The orientation results in Figs. 2(f) and 6(f) demonstrate that, when the capsule center coincides with the centerline, the capsule orientation is not equal to zero or $\pi/2$, i.e., the capsule shape is not exactly symmetric about the centerline. The NC04 capsule turns anticlockwise when approaching closely to the centerline, and even when staying near to the centerline after reaching it, as shown in Fig. 2(f). After reaching the centerline, the shape of the NC04 capsule is the least different from a circle as observed from Fig. 2(d), namely, the lengths of the semimajor and semiminor axes of its equimomental ellipse are almost the same, rendering the capsule easier to rotate. When the NC04 capsules stay near to the centerline, its a_{tt} decreases slowly, i.e., it undergoes clockwise membrane tank-treading motion, as observed from Fig. 5(a). Similar rotation and membrane tank-treading mo-

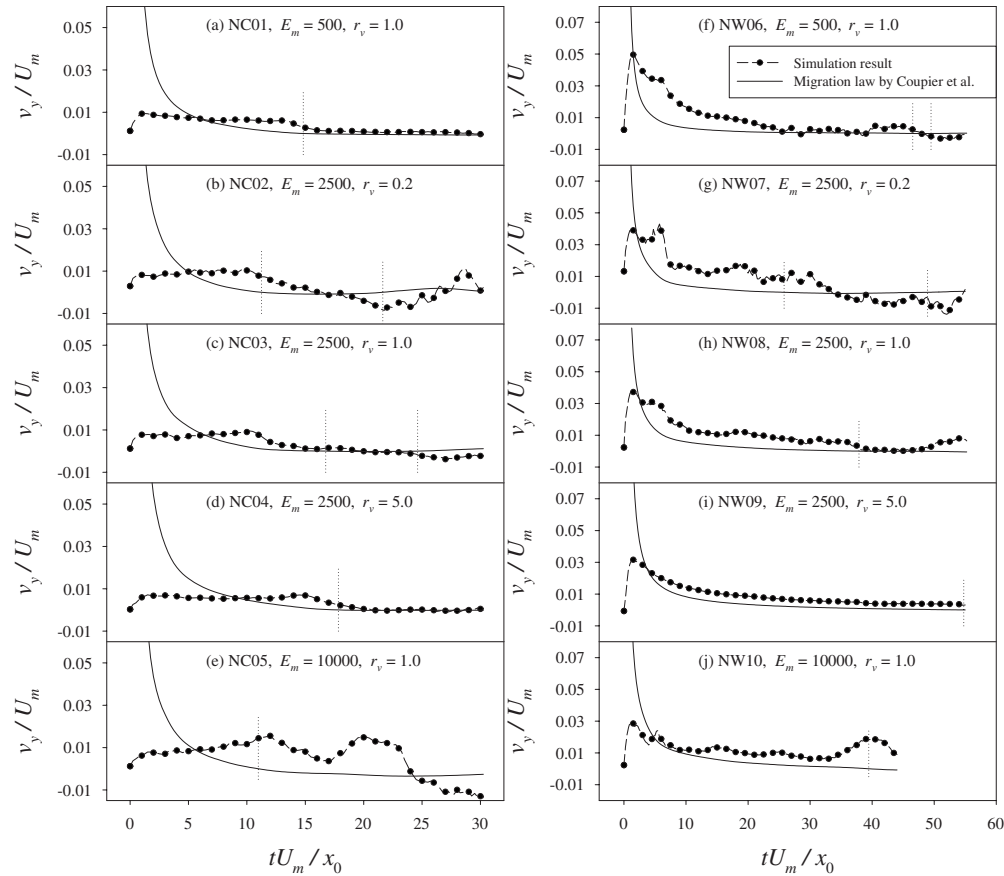


FIG. 9. Comparison between the temporal evolution of v_y from simulation in the present study with that by the migration law proposed by Couplier *et al.* [22]. Dotted line indicates the time at which the capsule centroid is on the centerline. In each plot, the results from the beginning to the first vertically dotted line are used for comparison, and the results from the first vertically dotted line to the end of the procedure are of no use.

tion are also observed for the NC03, NW06, and NW08 capsules when they stay near to the centerline, from Figs. 2(f), 6(f), 5(a), and 8. Kaoui *et al.* [24] discovered a slipper shape for vesicle when the reduced volume was lower than certain value, and found no slipper shape when the reduced volume was close to 1. The reduced volume in the present study is 1, and the results mentioned above show some similarity to the characteristics of the slipper shape, despite the distance between the capsule center and the centerline, and the tank-treading velocity are quite small.

Couplier *et al.* [22] experimentally and numerically investigated the cross-streamline noninertial migration of a vesicle in a bounded Poiseuille flow, and proposed a migration law where the lateral migration velocity is defined as a function of the vesicle center position and local shear rate of the unperturbed flow. The system studied by Couplier *et al.* [22] is different from that in the present study. Here the comparison between the two systems is conducted just as an attempt. Based on the nondimensionalization approach used in the present paper, the migration law can be expressed as

$$v_y^* = \frac{-\xi y^*}{0.96 \times 2^{\delta} (y^* - y_0^*)^{\delta}}, \quad (22)$$

where v_y^* is the nondimensional capsule velocity in y direction, and y^* is the nondimensional capsule center position in

y direction starting from y_0^* . Couplier *et al.* [22] studied the influence of reduced volume $v = V/[4\pi(S/4\pi)^{3/2}/3]$ on the vesicle behavior, where V and S are the volume and surface area of vesicle, and found $\xi = 1.2 \times 10^{-2} \pm 0.2 \times 10^{-2}$ and $\delta = 1 \pm 0.1$ in the range of $0.970 < v < 0.975$. Here, $v = 1$ because of the initially circular shape of the 2D capsule, and $\xi = 1.2 \times 10^{-2}$ and $\delta = 1$ are chosen. The migration law [Eq. (22)] is thus rewritten as

$$v_y^* = \frac{-y^*}{160(y^* - y_0^*)}. \quad (23)$$

The center position and center velocity in y direction of capsule for each case can be obtained by simulation. The temporal variation in v_y obtained from simulation is represented by dashed line with dots in Fig. 9. By substituting into Eq. (23) the capsule center position in y direction from simulation, the temporal evolution in v_y determined by the migration law [Eq. (23)] is represented by solid line in Fig. 9 for comparison. The vertical dotted line in each case in Fig. 9 indicates the time at which the capsule centroid coincides with the centerline. In each plot, the results from the beginning to the first vertically dotted line are used for comparison, and the results from the first vertically dotted line to the end of the procedure are of no use. It is seen that the rapid increase of v_y in the initial adjustment period is not covered

by the migration law [Eq. (23)]. The comparison between the capsule behavior from the present simulation and that by the migration law [Eq. (23)] shows that the behavioral agreement for the near-wall capsule is better than that for the near-center capsule. Among all the near-wall capsules, the best agreement occurs to the NW09 capsule with the intermediate membrane dilation modulus and the highest viscosity ratio. In spite of this good agreement, the migration law [Eq. (23)] by Coupier *et al.* [22] cannot exactly catch the behavior of the NW09 capsule, even adjusting the values of parameters ξ and δ . According to the migration law [Eq. (23)], v_y becomes zero when capsule centroid reaches the centerline. By the present simulation, however, the migration velocity of the NW09 capsule is not zero when the capsule centroid coincides with the centerline, as observed from the v_y curve shown in Fig. 6(b).

Apart from the membrane dilation modulus and the viscosity ratio, the initial position also influences the performance behavior of capsule. For example, the NC03 and NW08 capsules have the same mechanical properties. The difference in their lateral movements, shown in Figs. 2(a) and 6(a), clearly demonstrates the effect of initial capsule position on the capsule behavior. The NC03 capsule moves upward first, stays near to the centerline for a period, and then moves downward back to the lower half of microchannel, however, the NW08 capsule moves upward into the upper half of microchannel after staying near to the centerline for a period. Doddi and Bagchi [20] found that the motion of the capsule was quasisteady. They conducted two kinds of simulations. The first is the free capsule simulation, where the capsule is released near the bottom wall and the simulation stops until the capsule reaches closely to the centerline. The second is the quasisteady simulation, where an undeformed spherical capsule is released at different lateral locations along the trajectory of the free capsule, and the simulations stop just after the initial adjustment period is passed. Excellent agreement between the free capsule and the quasisteady capsule results were observed in terms of the migration velocity, slip velocity, deformation, and angular orientation. If the process is absolutely steady, the initial position of the capsule does not affect the capsule behavior. However, the quasisteady process does not necessarily mean the absolutely steady process. For capsules with different initial positions, small difference in capsule behavior shows up when capsules are not near to the microchannel centerline because the lateral migration process is quasisteady, but significant difference in capsule behavior can be observed when capsules approach closely to the centerline and after the capsules move across the centerline.

IV. CONCLUSION

The long-term lateral migration of 2D capsule in microchannel flow in cases with different initial capsule positions, membrane dilation moduli, and viscosity ratios is studied by simulation in the present paper. The numerical method used

in this paper combines a finite volume technique for solving the fluid problem on fixed Eulerian grid with a front tracking technique for capturing and tracking the capsule membrane discretized by Lagrangian nodes.

The near-center and near-wall capsules studied in the present paper experience tilting and membrane tank treading, and migrate laterally while moving along the surrounding flow. The lateral migration of capsule demonstrates the existence of lift effect of the surrounding flow. The effects of initial capsule position, membrane elastic dilation modulus, and viscosity ratio on capsule behavior can be observed clearly from the results in this paper. Before capsule approaches to the microchannel centerline closely, lower membrane dilation modulus and lower viscosity ratio tend to result in faster lateral migration. The initial position also influences the performance behavior of capsule. The difference in initial position brings about small difference in capsule behavior when capsule is not near to the microchannel centerline since the lateral migration of capsule is a quasisteady process, but might lead to significant difference in capsule behavior when capsule approaches closely to the centerline.

The lateral migration process of near-center capsule consists of two parts. After the initial adjustment period and before capsule approaches closely to the microchannel centerline, velocity in y direction, v_y , does not change much for a period, during which the capsule moves almost linearly with time in y direction, as shown in Figs. 2(b) and 2(a). This is the first part. In the second part, different capsules behave differently according to their mechanical properties, after they approach to the centerline closely. The lateral migration process of near-wall capsule consists of three parts. In the first part, namely just after the initial adjustment period, the capsule moves toward the centerline with relatively higher velocity, as shown in Figs. 6(a) and 6(b). The subsequent two parts for the near-wall capsule are somewhat similar to the two parts for the near-center capsule.

The lateral migration of capsule may be caused by various environmental conditions, for example, the presence of a wall, the nonlinearity of the shear flow such as the Poiseuille flow, and the nonlinear characteristic of the fluid. When the capsule is near to microchannel wall, the effect of the wall might dominate, leading to relatively faster lateral migration of capsule. When the capsule is not far away from the centerline, the effect of the nonlinearity of Poiseuille flow might dominate, resulting in relatively slower lateral movement of capsule. When capsule is located closely to the centerline, capsules behave differently, where the reason still remains poorly understood and it will be one of our future studies.

ACKNOWLEDGMENTS

The authors gratefully acknowledge the financial support from the Ministry of Education of Singapore through Academic Research Fund (AcRF) Tier 1 under the Project No. M52056029 (RGM 7/07).

- [1] R. Skalak and P. I. Branemark, *Science* **164**, 717 (1969).
- [2] T. W. Secomb and R. Hsu, *Biophys. J.* **71**, 1095 (1996).
- [3] C. Pozrikidis, *Phys. Fluids* **17**, 031503 (2005).
- [4] B. Lorz, R. Simson, J. Nardi, and E. Sackmann, *EPL* **51**, 468 (2000).
- [5] R. Skalak, N. Ozkaya, and T. C. Skalak, *Annu. Rev. Fluid Mech.* **21**, 167 (1989).
- [6] T. W. Secomb and R. Skalak, *Microvasc. Res.* **24**, 194 (1982).
- [7] D. Halpern and T. W. Secomb, *J. Fluid Mech.* **203**, 381 (1989).
- [8] C. Quéguiner and D. Barthes-Biesel, *J. Fluid Mech.* **348**, 349 (1997).
- [9] Y. Lefebvre and D. Barthes-Biesel, *J. Fluid Mech.* **589**, 157 (2007).
- [10] C. W. Hirt and B. D. Nichols, *J. Comput. Phys.* **39**, 201 (1981).
- [11] N. Ashgriz and J. Y. Poo, *J. Comput. Phys.* **93**, 449 (1991).
- [12] J. Glimm, J. Grove, B. Lindquist, O. A. McBryan, and G. Tryggvason, *SIAM (Soc. Ind. Appl. Math.) J. Sci. Stat. Comput.* **9**, 61 (1988).
- [13] S. O. Unverdi and G. Tryggvason, *J. Comput. Phys.* **100**, 25 (1992).
- [14] M. Abkarian, C. Lartigue, and A. Viallat, *Phys. Rev. Lett.* **88**, 068103 (2002).
- [15] S. Sukumaran and U. Seifert, *Phys. Rev. E* **64**, 011916 (2001).
- [16] I. Cantat and C. Misbah, *Phys. Rev. Lett.* **83**, 880 (1999).
- [17] U. Seifert, *Phys. Rev. Lett.* **83**, 876 (1999).
- [18] P. Olla, *J. Phys. A* **30**, 317 (1997).
- [19] N. Callens, C. Minetti, G. Coupier, M.-A. Mader, F. Dubois, C. Misbah, and T. Podgorski, *EPL* **83**, 24002 (2008).
- [20] S. K. Doddi and P. Bagchi, *Int. J. Multiphase Flow* **34**, 966 (2008).
- [21] B. Kaoui, G. H. Ristow, I. Cantat, C. Misbah, and W. Zimmermann, *Phys. Rev. E* **77**, 021903 (2008).
- [22] G. Coupier, B. Kaoui, T. Podgorski, and C. Misbah, *Phys. Fluids* **20**, 111702 (2008).
- [23] G. Danker, P. M. Vlahovska, and C. Misbah, *Phys. Rev. Lett.* **102**, 148102 (2009).
- [24] B. Kaoui, G. Biroso, and C. Misbah, *Phys. Rev. Lett.* **103**, 188101 (2009).
- [25] G. Ma, J. S. Hua, and H. Li, *Phys. Rev. E* **79**, 046710 (2009).
- [26] J. Hua and J. Lou, *J. Comput. Phys.* **222**, 769 (2007).
- [27] C. S. Peskin, *J. Comput. Phys.* **25**, 220 (1977).
- [28] C. Pozrikidis, in *Modeling and Simulation of Capsules and Biological Cells*, edited by C. Pozrikidis (CRC, Boca Raton, 2003).
- [29] C. Migliorini, Y. H. Qian, H. D. Chen, E. B. Brown, R. K. Jain, and L. L. Munn, *Biophys. J.* **83**, 1834 (2002).
- [30] G. A. Dunn and A. F. Brown, *J. Cell Sci.* **83**, 313 (1986).
- [31] J. Feng, H. H. Hu, and D. D. Joseph, *J. Fluid Mech.* **277**, 271 (1994).
- [32] C. E. Chaffey, H. Brenner, and S. G. Mason, *Rheol. Acta* **4**, 64 (1965).